Integrity assessment of impacted thick composite laminates using phased array ultrasonic testing

Nokhbatolfoghahai, Ali; Groves, Roger M.

Important note
To cite this publication, please use the final published version (if applicable).
Please check the document version above.

Integrity assessment of impacted thick composite laminates using phased array ultrasonic testing

6

Ali Nokhbatolfoghahai[1,2] and Roger M. Groves[2]
[1]Department of Aeronautics, Imperial College London, London, United Kingdom,
[2]Faculty of Aerospace Engineering, Aerospace Structures & Materials Department, Delft University of Technology, Delft, The Netherlands

6.1   Introduction

Fiber-reinforced polymer (FRP) composites play a pivotal role in modern industrial applications, offering a remarkable combination of strength, durability, and versatility. These materials are vital for enhancing the performance and longevity of various structures and components across industries such as aerospace, automotive, construction, and maritime. FRPs, comprising a matrix reinforced with high-strength fibers like carbon, glass, or aramid, provide exceptional strength-to-weight ratios, making them ideal for lightweight and high-performance applications. Furthermore, their corrosion resistance and design flexibility have revolutionized industrial engineering by reducing maintenance costs, improving energy efficiency, and expanding the possibilities for innovative designs.

Damages and defects may occur during the manufacturing or in-service use of composite structures. These defects and damages may vary in size, severity, and location (Fahr, 2014; Williams & Starke, 2003). Nondestructive testing (NDT) for FRPs holds paramount importance in ensuring the integrity and reliability of these materials in critical industrial applications. NDT techniques, such as ultrasound, radiography, thermography, and acoustic emission, are indispensable tools for detecting hidden defects, delaminations, voids, or degradation within FRPs without causing any damage to the material (Bossi & Giurgiutiu, 2015; Henrich & Schnars, 2006; Namkung et al., 2016; Steinchen et al., 1998; Heida & Platenkamp, 2011; Smith et al., 2013). These methods are vital in assessing the quality and reliability of FRP components, from aerospace components to wind turbine blades and civil infrastructure. Ensuring the proper function of NDT for FRPs not only minimizes the risk of catastrophic failures but also extends the service life of FRP structures and reduces maintenance costs (Bossi & Giurgiutiu, 2015).

The ultrasonic method is a highly valuable technique for Nondestructive evaluation (NDE) of FRP composites. Ultrasonic testing (UT) is an acoustic inspection technique measuring the reflection or transmission of pulsed elastic waves in engineering materials. The acoustic impedance mismatch between air, water, and structural solids (such as metals or composites) causes reflection, transmission, and

refraction of ultrasonic waves at interfaces. This phenomenon is exploited in ultrasonic testing for inspecting structural components and has made high-frequency ultrasound an attractive solution for the inspection of many of the defects in structural components (Ibrahim, 2014).

The significance of this method lies in its precision, providing detailed information about defect size, location, and nature, thus ensuring structural safety and reliability. It is highly sensitive, capable of detecting even small defects, and allows for the evaluation of flaws at varying depths within the material. Modern ultrasonic equipment provides real-time imaging, aiding in defect characterization. Moreover, it is nondestructive, preserving the integrity of the material being tested, and is versatile and applicable to a wide range of materials, including metals, composites, and plastics. However, there are certain limitations to consider, including the need for skilled operators to interpret results accurately, the requirement for surface preparation, potential limitations in accessibility for irregularly shaped or hard-to-reach areas, and reduced effectiveness in materials with extreme roughness or high attenuation levels (ASTM E2533-09 Standard Guide for Nondestructive Testing of Polymer Matrix Composites Used in Aerospace Applications, 2009).

UT encompasses several techniques that vary in their application, equipment, or the way sound waves are generated and analyzed. Here are some of the different ultrasonic techniques:

- **Pulse-echo technique:** This is the most common UT technique. It involves the transmission of a short pulse of ultrasound into a material. The system measures the time it takes for the pulse to reflect from internal boundaries or defects within the material. By analyzing the time delay and amplitude of the returned signals, technicians can determine the depth and size of the defect.
- **Through-transmission technique:** In this method, two transducers are used, one for transmitting the ultrasonic waves and the other for receiving them. The transmitting transducer sends a continuous wave of ultrasound through the material, and the receiving transducer on the other side detects the transmitted signal. This technique is useful for inspecting thicker materials and for detecting discontinuities in the entire thickness.
- **Phased array ultrasonics:** This advanced technique uses multiple small transducer elements that can be individually controlled and phased. By varying the timing and amplitude of the signals from each element, phased array systems can create and steer focused sound beams. This allows for more precise and flexible inspection of complex geometries.
- **Time-of-flight diffraction (TOFD):** TOFD is particularly effective in detecting and sizing cracks. It involves sending two ultrasonic waves from the same side of the material, one at an angle to the surface and another parallel to it. The time it takes for diffracted waves to reach the receiver is measured. TOFD provides excellent defect localization and sizing capabilities.
- **Guided wave ultrasonics:** This technique is suitable for inspecting long lengths of pipes or structures. Guided waves are ultrasonic waves that travel along the length of the structure, allowing for the screening of large areas with a single test. They are often used for corrosion and defect detection in pipelines (Nokhbatolfoghahai et al., 2020).
- **Immersion testing:** This technique involves immersing the material in water, which acts as a coupling medium between the transducer and the material. Immersion testing is commonly used for the inspection of aerospace and automotive components.

Each of these UT techniques has its specific strengths and applications, making them valuable tools in various industries for ensuring the quality and integrity of materials and structures. The choice of technique depends on the specific inspection requirements, material characteristics, and the nature of the defects being targeted.

6.2 Basic theories

6.2.1 Elastic waves

An acoustic wave is composed of oscillations of discrete particles of material. An elastic wave is a wave that propagates in solids and is dependent on the properties of the solids. The elastic wave propagation is given by Eq. (6.1) (Williams & Starke, 2003)

$$\mu\nabla^2\mathbf{u} + (\lambda + \mu)\nabla(\nabla.\mathbf{u}) - \rho\frac{\partial^2\mathbf{u}}{\partial t^2} = 0 \tag{6.1}$$

where $\mathbf{u}$ is the particle displacement vector, μ and λ are Lame's constants and t is time. When the particles oscillate in the direction of the propagation of the wave, the wave is called a longitudinal wave (P-wave). Since compressional and dilatational forces are active in the wave, it is also called a compression wave or a pressure wave. This is a real sound wave because it can transmit the oscillations of a source of acoustic energy through the air to our ears. The same wave also transmits sound through liquid or solid bodies. However, in solid bodies, another kind of wave may also occur. This wave is called a transverse wave or shear wave (S-wave) as the particles no longer oscillate in the direction of propagation of the wave but at right angles to it. The direction of oscillation of particle is called the polarization of the waves. Fig. 6.1 shows the schematic shape of the propagation of an S-wave and a P-wave. Since liquids and gases are incapable of transmitting shear, transverse waves cannot travel through them (Krautkrämer & Krautkrämer, 2013). S-waves and P-waves have different velocities, and the longitudinal wave velocity is typically more than twice the shear wave velocity in metals.

The waves described above are for infinite medium and are not restricted by the size or shape of the medium of propagation. For finite bodies, different waves can be defined by the deformation of the bodies. Some of these waves are surface or Rayleigh waves (Su & Ye, 2009) which propagate on the surface of a flat or curved medium. When a solid medium is further limited in size to a finite thickness, a pure surface wave cannot exist unless its wavelength is much smaller than the thickness of the plate. In such a solid, we have Lamb waves which propagate along the wave with particles oscillating perpendicular to the direction of propagation. Lamb waves are also called guided waves and are of symmetrical and asymmetrical modes (Su & Ye, 2009). The reflection and transmission of waves impinging an interface between two materials depends on the acoustic impedance of the materials and the angle of incidence. Acoustic wave impedance is a property of a material that
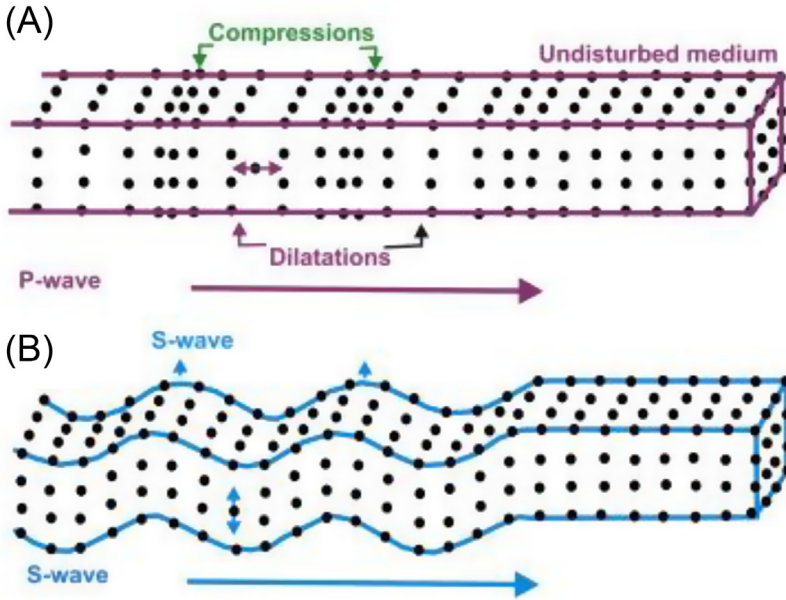
Figure 6.1 A schematic shape of wave propagation for (A) longitudinal wave and
(B) transverse wave.
Source: From Moon, C.J., Whateley, M.K., & Evans, A.M. (2006). *Introduction to mineral
exploration* (No. Ed. 2). Blackwell publishing. (Original work published 2006).

provides the resistance of the material to the propagation of a wave through it. The
different acoustic impedances of materials cause reflection and transmission of
waves at the interface between one material to another. Furthermore, elastic wave
propagation is complicated by the fact that mode conversion occurs at a nonnormal
angle of incidence, and also that reflection/refraction occurs at discontinuities inside
a test object. In mode conversion, a longitudinal wave impinging at an interface
will be converted to a shear wave or vice-versa depending on the acoustic imped-
ance mismatch between the two materials.

A typical example of mode conversion in NDE imaging is the multiple mode
conversion that can occur at cracks (Ogilvy & Temple, 1983). There, mode conver-
sion generates both longitudinal and shear-diffracted waves at the tip of the crack.
A surface wave may also be generated along the crack, which has a different speed
and hence will result in additional diffracted waves at the crack tips (Tittmann,
1983). The resulting signals will then consist of a mix of different wave modes
which will be very difficult to discriminate.

6.2.2 Attenuation and impedance

One of the important features when the pulse travels into the material is the
attenuation. Ultrasonic wave attenuation is the reduction in amplitude of an

ultrasonic wave as it propagates through a medium. It is caused by a variety of factors, including:

- **Absorption:** Absorption is the conversion of ultrasonic energy into heat energy. This is caused by the interaction of the ultrasonic wave with the molecules of the medium. Absorption is typically higher at higher frequencies and in more viscous media.
- **Scattering:** Scattering is the deflection of ultrasonic waves from their original path. This can be caused by irregularities in the medium, such as particles, voids, and cracks. Scattering is typically higher at higher frequencies and in more heterogeneous media.
- **Beam spreading:** Beam spreading is the divergence of an ultrasonic beam as it propagates through a medium. This is due to the diffraction of the wave. Beam spreading is typically higher at higher frequencies and for longer propagation distances.

The attenuation of ultrasonic waves can be expressed as $A(z) = A(0)e^{(-\alpha z)}$ where $A(z)$ is the amplitude of the ultrasonic wave at a distance z from the source, $A(0)$ is the amplitude of the ultrasonic wave at the source and α is the attenuation coefficient (Cawley, 2006; Schmerr, 2016b). The attenuation coefficient is a measure of the rate at which the ultrasonic wave is attenuated. The most common unit for that is decibels per meter (dB/m) and its relationship is $I = 20\log\left(\frac{A}{A_0}\right)$. Ultrasonic wave attenuation is an important factor to consider in the design and application of ultrasonic devices.

Acoustic impedance is a material property that is defined as the product of the material's density and acoustic velocity. It is a measure of how well a material transmits sound waves and it is an important parameter in ultrasonic nondestructive testing because it affects the transmission and reflection of ultrasonic waves at interfaces between different materials. Acoustic impedance is calculated as $Z = \rho V$ where Z is the acoustic impedance in Pascals-seconds per meter (Pa $\cdot$ s/m), ρ is the density in kilograms per cubic meter (kg/m^3) and V is the acoustic velocity in meters per second (m/s) (Blitz & Simpson, 1995). When an ultrasonic wave encounters an interface between two materials with different acoustic impedances, some of the wave will be transmitted into the second material and some of the wave will be reflected back into the first material. The amplitudes of the waves that are transmitted and reflected depends on the difference in acoustic impedance between the two materials. The percentage of the reflected energy is calculated as $R = \left(\frac{Z_1 - Z_2}{Z_1 + Z_2}\right)^2 \times 100$ and the percentage of energy that is transmitted is $T = \left(\frac{2Z_1 Z_2}{Z_1 + Z_2}\right)^2 \times 100$ where Z_1 and Z_1 are the acoustic impedances of the two materials.

In ultrasonic NDT, ultrasonic waves are used to detect defects in materials, such as cracks, voids, and delaminations. The acoustic impedance of the defect is typically different from the acoustic impedance of the surrounding material. This difference in acoustic impedance causes the ultrasonic wave to be reflected from the defect. The reflected ultrasonic wave can be detected by the transducer and used to determine the location and size of the defect. Acoustic impedance is also used in ultrasonic NDT to measure the thickness of materials. In this application, the

ultrasonic wave is reflected from the back surface of the material. The time it takes for the reflected ultrasonic wave to return to the transducer can be used to calculate the thickness of the material.

6.2.3   Refraction and mode conversion

Refraction and mode conversion are two important phenomena that occur in ultrasonic nondestructive testing.

Refraction is the bending of an ultrasonic wave as it travels from one medium to another with a different acoustic velocity. The angle of refraction is determined by the acoustic velocities of the two media and the angle of incidence of the ultrasonic wave. Snell's law is a mathematical describes the relationship between the angle of incidence, the angle of refraction, and the acoustic velocities of the two media. Snell's law is as follows (Blitz & Simpson, 1995):

$$V_1 \sin \theta_1 = V_2 \sin \theta_2 \tag{6.2}$$

where V_1 and V_2 are the ultrasonic wave velocities in the first and second medium, respectively, and θ_1 and θ_2 are the angle of incidence and angle of refraction respectively. In ultrasonic NDT, refraction is used to:

- Focus the ultrasonic beam on the region of interest. This is often done using angle beam ultrasonic testing (AUT) or phased array ultrasonic testing (PAUT).
- Detect defects that are hidden from the direct path of the ultrasonic beam. For example, a defect in a weld may be hidden from the direct path of the ultrasonic beam, but it may be detected by a refracted ultrasonic wave.
- Characterize the properties of materials. For example, shear wave UT can be used to measure the shear modulus of a material by measuring the angle of refraction of a shear wave.

Refraction is an important phenomenon in ultrasonic NDT because it allows ultrasonic waves to be used to inspect complex geometries and to detect defects that would be difficult or impossible to detect with other methods. Using Snell's law allows the inspector to position the transducer at the correct angle to inspect the desired region of the material.

Mode conversion is the conversion of one type of ultrasonic wave to another type of ultrasonic wave. The two most common types of ultrasonic waves are longitudinal waves and shear waves. Mode conversion can occur at any interface between two materials with different acoustic impedances. When an ultrasonic wave encounters an interface between two materials with different acoustic impedances, in addition to transmission and reflection, some of the ultrasonic waves may also be converted to a different type of ultrasonic wave at the interface. Also, when an ultrasonic wave travels through a composite material, it can encounter a variety of interfaces, such as the interfaces between the fiber and matrix phases, between different layers of the composite, and between the composite and any surrounding materials. At each interface, the ultrasonic wave can be transmitted, reflected, and converted to a different mode of wave.

Mode conversion can be used to improve the sensitivity of ultrasonic NDT of composite materials by generating shear waves in the material. Shear waves are more sensitive to certain types of defects in composite materials, such as fiber breakage, delamination, and matrix cracking. Mode conversion can also be used to detect defects that are hidden from the direct path of the ultrasonic beam. For example, a defect in a composite laminate may be hidden from the direct path of the ultrasonic beam, but it may be detected by a converted shear wave.

Here are some examples of how mode conversion is used in ultrasonic NDT of composite materials:

- AUT is often used to inspect composite laminates for defects. The transducer is positioned at an angle to the surface of the laminate, which generates an ultrasonic beam that is refracted and converted to a shear wave and the converted shear wave can then be used to inspect the laminate for defects.
- PAUT can be used to generate multiple ultrasonic beams that are refracted and converted to shear waves at different angles. This allows for the inspection of large areas and for the detection of defects that are hidden from the direct path of the ultrasonic beam.
- Characterize the properties of materials. For example, shear wave UT can be used to measure the shear modulus of a material by measuring the velocity of a converted shear wave.

Mode conversion is a powerful tool that is used in ultrasonic NDT to improve the sensitivity, reliability, and versatility of UT. Fig. 6.2 shows how the incident angle affects the relative amplitude of wave modes.
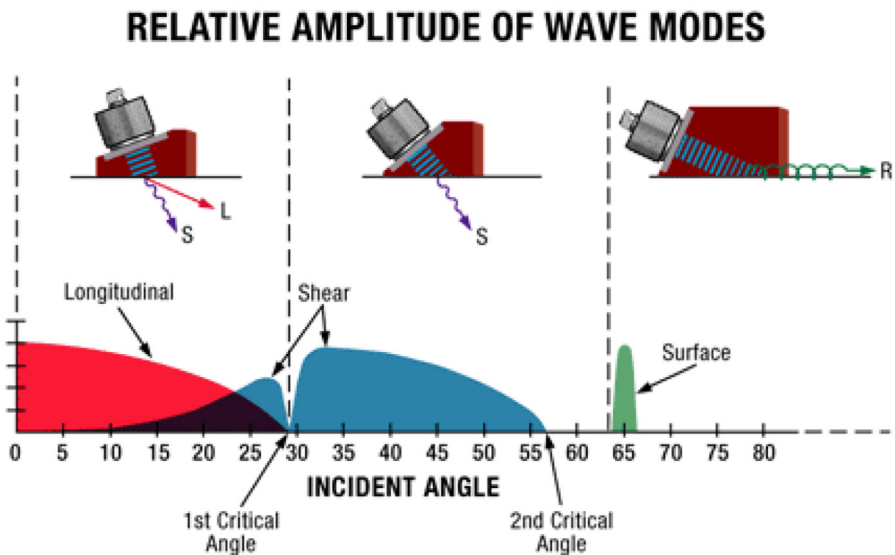

Figure 6.2 The relative amplitude of wave modes with respect to incident angle.
Source: From OLYMPUS. (2024). https://www.olympus-ims.com/.

6.2.4　Scattering from defects

Ultrasonic waves can be used to detect defects in materials by measuring the time it takes for the waves to travel through the material and the amplitude of the reflected waves. Defects in materials can cause ultrasonic waves to be scattered, absorbed, or refracted. The scattering of ultrasonic waves by defects is the most common mechanism used to detect defects in ultrasonic NDT. When an ultrasonic wave encounters a defect, such as a crack, void, or delamination, the wave will be scattered in different directions. Larger defects will scatter more ultrasonic waves than smaller defects. Defects with sharp edges or corners will also scatter more ultrasonic waves than defects with smooth edges. The following are some of the main mechanisms by which ultrasonic waves scatter from composite defects (Ono, 2020; Yin et al., 2018):

- **Rayleigh scattering:** Rayleigh scattering is a type of scattering that occurs when the wavelength of the ultrasonic wave is much larger than the size of the defect. In this case, the defect acts as a small point scatterer and the ultrasonic wave is scattered in all directions.
- **Mie scattering:** Mie scattering is a type of scattering that occurs when the wavelength of the ultrasonic wave is comparable to the size of the defect. In this case, the ultrasonic wave is scattered in a complex pattern that depends on the size, shape, and orientation of the defect.
- **Geometric scattering:** Geometric scattering is a type of scattering that occurs when the wavelength of the ultrasonic wave is much smaller than the size of the defect. In this case, the ultrasonic wave is scattered in a specular direction, like light reflecting from a mirror.

The scattering of ultrasonic waves from composite defects can be measured using a variety of UT techniques, such as pulse-echo UT, through-transmission ultrasonic testing (TUT), and PAUT.

The scattering of ultrasonic waves from defects can be modeled using a variety of mathematical methods, such as the Rayleigh−Sommerfeld diffraction integral (Schmerr, 2003) and the Kirchhoff approximation (Huang, 2006; Lopez-Sanchez et al., 2006; Schmerr, 2016a). These models can be used to predict the amplitude and frequency spectrum of the scattered waves for a given defect.

6.2.5　Distinguishing different damage mechanisms in composite laminates using ultrasonic testing

Delamination, matrix cracking, and fiber breakage are three common types of defects in composite materials. These defects can all cause ultrasonic waves to scatter, but the scattering patterns will be different for each type of defect. Here is a summary of the scattering characteristics of each type of defect:

- **Delamination:** Delamination is the separation of two layers of a composite material. Delaminations typically cause a significant amount of scattering, especially at low frequencies. The scattering pattern from delamination is typically diffuse, meaning that the scattered waves are scattered in all directions.

- **Matrix cracking:** Matrix cracking is the formation of cracks in the matrix of a composite material. Matrix cracks typically cause less scattering than delaminations, and the scattering pattern is typically more directional. The scattered waves from matrix cracks are typically scattered in the direction of the crack.
- **Fiber breakage:** Fiber breakage is the failure of individual fibers in a composite material. Fiber breakage typically causes very little scattering, and the scattering pattern is typically very directional. The scattered waves from fiber breaks are typically scattered in the direction of the broken fiber.

Therefore, by analyzing the scattering pattern of ultrasonic waves, it is possible to distinguish between delamination, matrix cracking, and fiber breakage. Here are some specific examples of how different UT techniques use the scattering pattern of the ultrasonic waves to distinguish between these three types of defects:

- AUT can be used to detect delaminations and matrix cracks. The scattering pattern from a delamination will typically be diffuse, while the scattering pattern from a matrix crack will typically be more directional.
- PAUT can be used to image delaminations and matrix cracks based on wave scattering due to defects (or any discontinuity). PAUT can be used to create cross-sectional images of the material, which can help to identify the location, size, and shape of the defect.
- TUT can be used to distinguish delamination and fiber breakage. The scattering from delamination will typically cause significant attenuation of the transmitted signal, while the scattering from fiber breakage will typically cause a much smaller attenuation.

In addition to these three basic techniques, there are some other techniques that can be used to distinguish between delamination, matrix cracking, and fiber breakage. These techniques include:

- **Frequency dependence of scattering:** The scattering from delaminations is typically less frequency-dependent than the scattering from matrix cracks and fiber breaks. This means that the scattering from delaminations will be similar at all frequencies, while the scattering from matrix cracks and fiber breaks will increase with frequency.
- **Polarization dependence of scattering:** The scattering from delaminations and fiber breaks is typically polarization-dependent, while the scattering from matrix cracks is typically polarization-independent. This means that the scattering from delaminations and fiber breaks will vary depending on the polarization of the incident ultrasonic wave.
- **Wave mode conversion:** Delaminations and matrix cracks can both cause ultrasonic waves to convert from one mode to another. For example, a longitudinal wave may be converted to a shear wave at a delamination or a matrix crack. The mode conversion is typically more significant for delaminations than for matrix cracks.

By combining these different techniques, it is possible to distinguish between delamination, matrix cracking, and fiber breakage in composite materials.

6.3 Phased array ultrasonic testing

PAUT is a powerful tool for damage assessment in thick composite laminates. It offers several advantages over other nondestructive testing methods, such as

conventional UT and radiographic testing (RT). PAUT systems use multiple transducer elements that can be controlled independently to generate and steer ultrasonic beams (see Fig. 6.3). This allows for the inspection of complex geometries and the detection of small defects.

PAUT emerged in the 1960s, initially for medical applications. It was not until the 1980s that PAUT began to be used for nondestructive testing. PAUT quickly gained popularity in the NDT industry due to its many advantages over conventional UT methods (Schmerr, 2003). Conventional UT typically uses single-element transducers that produce a fixed beam angle, limiting the depth of focus and beam coverage. In contrast, PAUT employs a multielement array, allowing for beam steering, focusing, and control over the inspection process. This adaptability is crucial in achieving better defect detection, particularly in complex structures or materials like thick composite laminates, where varied orientations and complex geometries pose challenges for traditional methods. PAUT enables the generation of multiple focal points, providing enhanced resolution, improved signal-to-noise ratios, and the ability to inspect various areas simultaneously (Von Ramm & Smith, 1983). The flexibility and capability to adapt to different material properties and thicknesses significantly contribute to the reliability and accuracy of flaw detection. Additionally, PAUT allows for real-time visualization and imaging of internal structures, offering comprehensive data analysis, which is often limited in conventional methods. Table 6.1 provides a comparative analysis of PAUT with conventional UT methods (Von Ramm & Smith, 1983).

6.3.1 Principles and basics of phased array ultrasonic testing

PAUT systems generate ultrasonic waves by applying a voltage pulse to the transducer elements. The voltage pulse causes the transducer elements to vibrate, which generates ultrasonic waves. The frequency of the ultrasonic waves is determined by
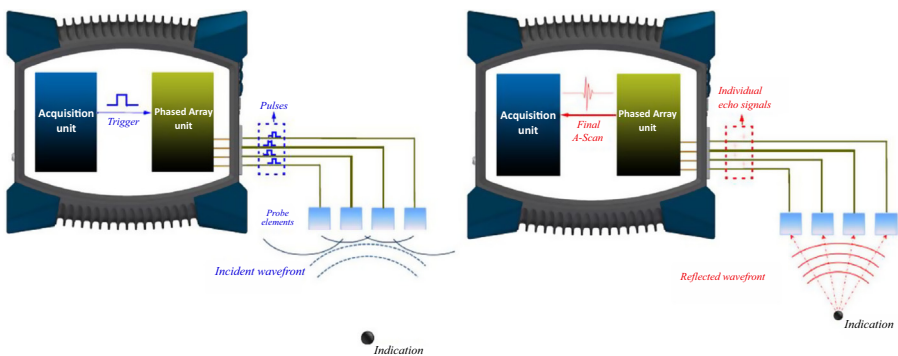

Figure 6.3 Transmitting and receiving signals using a phased array ultrasonic system. *Source*: From Tremblay, D.R. (2012). *Development and validation of a full matrix capture solution* (pp. 457−466). (Original work published 2012).

Table 6.1 Comparison of phased array ultrasonic testing and conventional ultrasonic testing methods.

Characteristic	Phased array ultrasonics (PAUT)	Conventional ultrasonic testing (UT)
Beam generation	Electronic	Mechanical
Beam steering	Electronic	Mechanical
Inspection speed	Fast	Slow
Inspection accuracy	High	Moderate
Defect detection capability	High	Moderate
Cost	High	Moderate

the natural frequency of the transducer elements. The ultrasonic waves propagate through the material being inspected and are reflected by defects in the material. The reflected ultrasonic waves are received by the transducer elements and converted back into electrical signals. The electrical signals are then processed by the PAUT system to generate images and data about the defects in the material (Mailloux, 1982).

The transducer array is typically arranged in a linear or matrix configuration. Linear arrays are used to generate one-dimensional beams, while matrix arrays are used to generate two-dimensional beams. The beam steering capability of PAUT is achieved by varying the time delay between the excitation of the transducer elements. By varying the time delay, the interference between the ultrasonic waves from the individual transducer elements can be constructive or destructive. Constructive interference will amplify the beam in a particular direction, while destructive interference will cancel out the beam in that direction (Von Ramm & Smith, 1983). The key components and functionalities of a phased array system are probes, software, and control mechanisms.

6.3.1.1 Probes

PAUT probes are typically designed for specific applications. For example, there are PAUT probes for inspecting welds, aerospace components, and composite materials. PAUT probes can have a variety of transducer configurations, such as linear arrays, matrix arrays, and sector arrays. The probes are typically coupled to the material being inspected using a couplant, such as water or gel. The design and configuration of these probes play a crucial role in determining the coverage and resolution of the inspection. Phased array probes can be categorized by type as follows:

- **Type:** Phased array transducers are designed for use with wedges that provide angle beam-type, zero angle, or delay line. Direct contact and immersion transducers are also available.
- **Frequency (penetration vs resolution):** Phased array transducers are available in a variety of frequencies, ranging from a few megahertz to several tens of megahertz. The frequency of the transducer determines the penetration depth and resolution of the inspection. Lower frequency transducers have greater penetration depth, but lower resolution. Higher frequency transducers have lower penetration depth, but higher resolution.
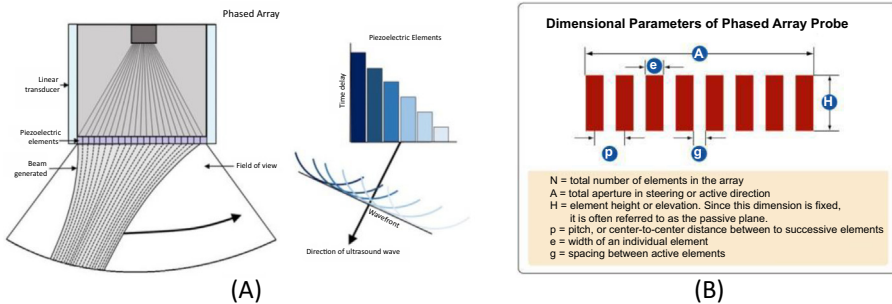
Figure 6.4 Diagram of (A) linear ultrasound phased array transducer. (B) Dimensional parameters of Phased array probe.
Source: From Nightingale (2017). https://doi.org/10.53347/RID-54646 and Olympus Phased Array Tutorial (2023). (Original work published 2023).

- **Number of elements (focusing and steering):** Phased array transducers can have any- where from a few to hundreds of elements. The number of elements in the transducer determines the beam steering capability and coverage area. More elements allow for more precise beam steering and larger coverage areas.
- **Size of elements (beam steering vs area coverage):** The size of the elements in a phased array transducer also affects the beam steering capability and coverage area. Smaller ele- ments allow for more precise beam steering, but larger elements are required for larger coverage areas.

The dimensional parameters of a phased array probe are defined in Fig. 6.4.

6.3.1.2   Software

PAUT software is a critical component of the PAUT system. The software used in PAUT systems allows for the control and manipulation of the ultrasonic beams. It enables operators to define the angle, focal point, and depth of the ultrasonic waves and provides real-time visualization and analysis of the collected data. PAUT soft- ware typically includes features such as C-scanning, B-scanning, and flaw detection.

6.3.1.3   Control mechanisms

These mechanisms are essential for the precise control of the timing and phase of ultrasonic waves emitted by each transducer element. Control mechanisms ensure the synchronization and coordination required for steering and focusing the ultra- sonic beams, ultimately enhancing the inspection's accuracy and effectiveness.

6.3.2   Phased array ultrasonic data acquisition

Data acquisition methods in PAUT are crucial for capturing and processing the ultrasonic signals that reveal the internal structural features and integrity of the

material being inspected. These methods play a significant role in determining the quality and accuracy of PAUT inspections.

6.3.2.1 Full matrix capture

This method is a comprehensive data acquisition method that captures the entire set of transmit-receive combinations between all transducer elements in a phased array (see Fig. 6.5). This results in a vast matrix of ultrasonic data that represents the complete interaction of the ultrasonic waves with the material. Full matrix capture (FMC) offers several advantages over traditional data acquisition methods, such as providing the highest possible resolution in PAUT, allowing for optimal dynamic focusing of the ultrasonic beam, etc. However it has some limitations such as generating a large amount of data, which requires more memory and processing capability, and it can be time-consuming due to the extensive volume of acquired data.

6.3.2.2 Linear scanning

This method involves firing the transducer elements in a phased array simultaneously, generating a single ultrasonic beam that travels in a straight line (see Fig. 6.6). It involves sequentially scanning a linear array of transducer elements across the surface of the material. The probe emits beams in a linear direction and receives reflections to create an image. Linear scanning is well-suited for inspecting materials with simple geometries and for applications where a focused beam is not required. It is also a relatively fast method, making it suitable for inspecting large areas.

6.3.2.3 Sectoral scanning

This method employs phased array transducers to sweep the beam through a range of angles, typically in a sector-shaped pattern (see Fig. 6.6). The beams are steered electronically by adjusting the time delays between the excitation of the individual
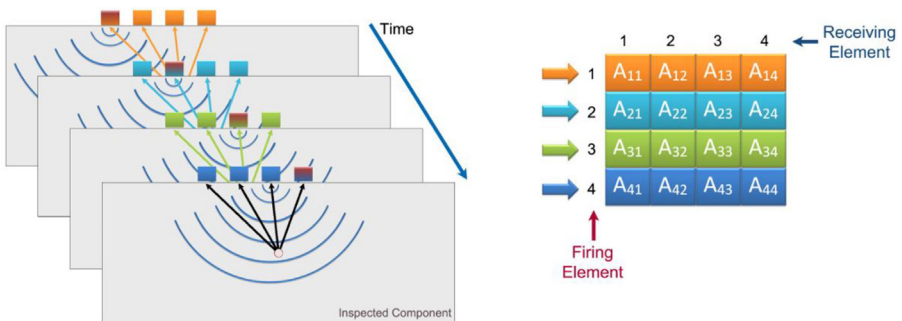

Figure 6.5 Full matrix capture principle.
Source: From Tremblay, D. R. (2012). *Development and validation of a full matrix capture solution* (pp. 457−466). (Original work published 2012).
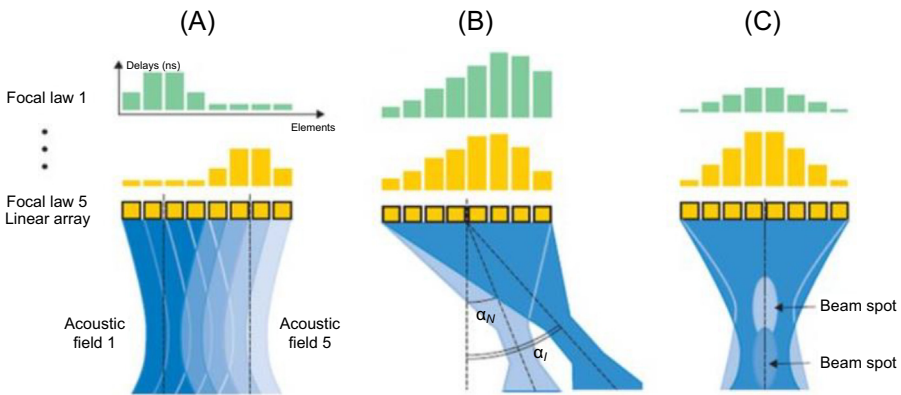
Figure 6.6 Schematics of type of electric scanning: (A) linear scanning, (B) sectorial scanning, and (C) focusing scanning.
Source: From Dubee, N., & Michael, D. C. H. (2007). *Advances in phased array ultarasonic applications*. Technical note. Technical Communications Services. Olympus NDT. (Original work published 2007).

transducer elements. Sectoral scanning offers flexibility in steering and focusing the beam, making it suitable for inspecting complex shapes and welds and it can cover a broader area compared to linear scanning.

6.3.2.4 Raster scanning

Raster scanning involves moving the transducer array in a raster pattern across the surface of the material being inspected (see Fig. 6.7). For each position of the transducer array, a series of ultrasonic beams is fired, and the reflected signals are recorded. This method provides more comprehensive coverage of the inspected area compared to linear and sectoral scanning and is particularly useful for inspecting large and flat surfaces or materials. However, raster scanning also has some limitations such as being time-consuming and generating large data volumes.

6.3.3 Phased array ultrasonic views (scan)

In addition to different data acquisition methods, there are also different ultrasonic views which are defined by different plane views between the ultrasonic path and scanning parameters (scan or index axis). The most important views are presented in Fig. 6.8.

6.3.3.1 A-scanning

An A-scan, also known as an amplitude scan is a one-dimensional ultrasonic scan that is a representation of the received ultrasonic pulse amplitude versus time of
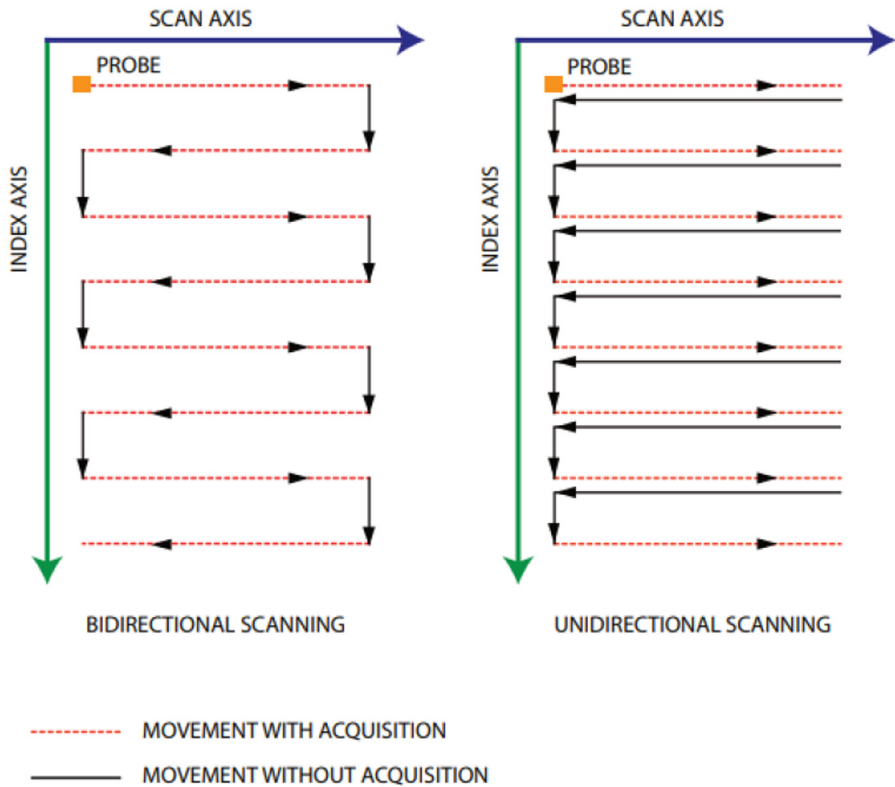
Figure 6.7 Bidirectional raster scanning (left) and unidirectional raster scanning (right).
Source: From Dubee, N., & Michael, D. C. H. (2007). *Advances in phased array ultarasonic applications*. Technical note. Technical Communications Services. Olympus NDT. (Original work published 2007).

flight or ultrasonic path, also called a waveform. A-scans are used to identify and characterize defects in materials, such as cracks, voids, and delaminations.

6.3.3.2 B-scanning

B-scanning is a method of data acquisition that generates a cross-sectional image of the inspected material. The B-scan is defined by the depth and probe movement axis. It involves firing a single ultrasonic beam and recording the reflected signals as the beam is moved along a line. The reflected signals are used to reconstruct a two-dimensional image of the material along the scan line. B-scanning provides detailed images of the cross-section of the material, allowing for precise defect location and characterization. However, B-scanning only provides information along the scan line, requiring multiple scans to inspect a large area. This method is a valuable tool for inspecting materials with known defects or for providing a detailed view of specific areas of interest.
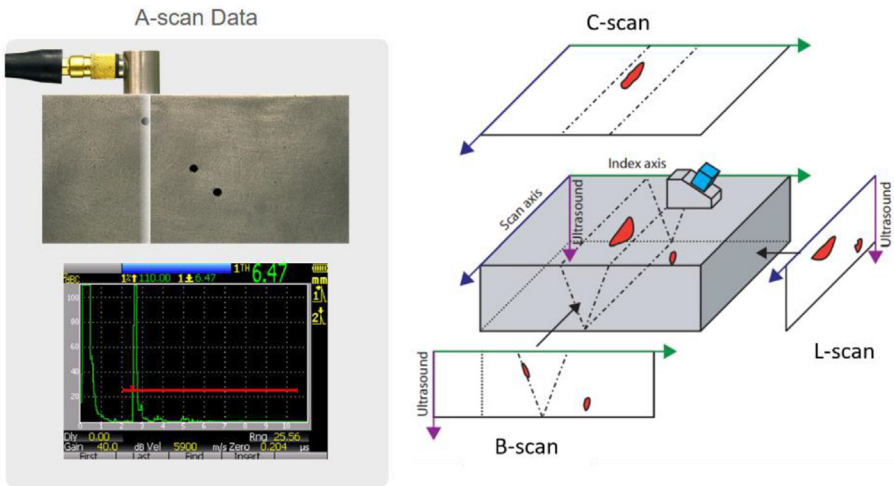
Figure 6.8 Ultrasonic A-scan, B-scan, L-scan, and C-scan.
Source: From Olympus Phased Array Tutorial (2023). (Original work published 2023).

6.3.3.3   L-scanning

In linear phased array ultrasonic NDT systems, an L-scan is a two-dimensional ultrasonic scan that is obtained by sweeping the ultrasonic beam across a surface using a linear array transducer and is defined by the depth and the electronic scan axis. The transducer consists of a series of closely spaced piezoelectric elements that are electronically controlled to emit and receive ultrasonic pulses. The beam is steered by electronically delaying the signals from the different elements, causing them to arrive at the target at slightly different times.

6.3.3.4   C-scanning

C-scanning is a method of data acquisition that generates a plan-view image of the inspected material. It involves firing a series of ultrasonic beams and recording the reflected signals for each beam. The reflected signals are used to reconstruct a two-dimensional image of the material's surface, similar to a photograph. C-scanning provides a comprehensive image of the entire inspected surface, enabling quick identification of defects or anomalies. C-scan images are easy to visualize and interpret, making them suitable for quick assessments. However, there are some limitations in using C-scan such as C-scanning only provides information about the average attenuation in the depth and information about depth of defects is not presented. Also, sometimes larger defects can create shadowing effects, hiding smaller defects behind them. C-scanning is a useful tool for inspecting large, flat surfaces or for providing a general overview of the condition of the material. It is commonly used for initial inspections to identify areas of interest that may require further examination using B-scanning or other methods. Ultrasonic A-scan, B-scan, L-scan, and C-scan are shown in Fig. 6.8.

The selection of the appropriate data acquisition method in PAUT depends on several factors, including the size and geometry of the material, the type of defects being inspected, and the desired level of detail. In some cases, a combination of data acquisition methods may be used to achieve the desired results. For example, C-scanning may be used to provide a general overview of the material, followed by B-scanning or FMC to focus on specific areas of interest. The selection of the appropriate data acquisition method is an important step in ensuring a successful PAUT inspection. By carefully considering the specific requirements of the inspection, the most suitable method can be chosen to maximize the quality and accuracy of the inspection results.

6.3.4   Phased array ultrasonic beamforming methods

In addition to data acquisition methods, beamforming algorithms are also a crucial component of PAUT, enabling precise control of the ultrasonic beam's direction, size, and shape. These algorithms determine how the individual transducer elements in a phased array are excited to generate and steer the ultrasonic beam.

Beamforming algorithms operate by manipulating the timing and amplitude of the electrical signals applied to each transducer element. By carefully controlling these parameters, the interference between the ultrasonic waves generated by each element can be constructively or destructively controlled. Constructive interference occurs when the waves from multiple elements arrive at a particular point in phase, resulting in reinforcement and amplification of the beam. Conversely, destructive interference occurs when the waves arrive out of phase, canceling each other out and reducing the beam intensity. By strategically controlling the timing and amplitude of the signals, beamforming algorithms can shape the ultrasonic beam into various forms, including focused beams, wide beams, and steered beams.

Several beamforming algorithms are commonly used in PAUT, each with its own strengths and limitations. Here are some of the most widely used algorithms:

Delay-and-sum (DAS) beamforming: DAS is the simplest beamforming algorithm and is widely used in PAUT systems. It achieves beam steering by introducing time delays between the signals applied to each transducer element. The time delays are calculated based on the desired beam direction. More information about this algorithm can be found in (Perrot et al., 2021).

Dynamic focusing (DF) beamforming: DF is an adaptive beamforming algorithm that continuously adjusts the beamforming parameters based on the received ultrasonic signals. This algorithm is particularly useful for inspecting complex geometries or materials with varying properties. More information about this algorithm can be found in Song and Greenleaf (1994).

Total focusing method (TFM): TFM is an image reconstruction technique that utilizes the FMC data to create a fully focused image of the inspected material. It applies beamforming principles to each pixel in the image, effectively focusing the ultrasonic beam at every point in the reconstruction area. By combining FMC and TFM, PAUT systems can achieve significantly higher resolution and sensitivity compared to traditional PAUT methods. This makes them particularly well-suited

for inspecting complex geometries, detecting small defects, and characterizing the size, shape, and orientation of defects. More information about this algorithm can be found in (Zhang et al., 2010).

Synthetic aperture focusing technique (SAFT): SAFT is a postprocessing beamforming technique that creates a focused image from multiple unfocused scans. This algorithm is particularly useful for inspecting large areas or materials with irregular surfaces. More information about this algorithm can be found in (Schmitz et al., 2000).

Beamforming algorithms control the direction, size, and shape of the ultrasonic beam by manipulating the interference between the waves from individual transducer elements as follows:

Direction control: To steer the beam in a particular direction, the time delays between the signals are adjusted such that constructive interference occurs in the desired direction.

Size control: The size of the beam is controlled by adjusting the number of transducer elements contributing to the beam. Fewer elements result in a wider beam, while more elements result in a narrower beam.

Shape control: The shape of the beam can be controlled by adjusting the amplitude distribution across the transducer array. Different amplitude distributions can create focused beams, wide beams, or beams with specific side-lobe patterns.

Case Studie: Sparcap and Skin Debonding Detection in Wind Turbine Blades

This section presents a case study exploring the challenges and limitations encountered during real-world ultrasonic inspection of a thick composite structure in an industrial setting. Through this case study, we not only identify these inherent obstacles but also propose a novel approach to address some of them. Additionally, we showcase various types of ultrasonic results to familiarize the reader with the typical outcomes a phased array ultrasonic inspection produces for this specific application.

The case study presented hereafter is a part of the smart maintenance innovation project AIRTuB: Automatic Inspection and Repair of Turbine Blades aims to develop a drone-based system that provides leading-edge erosion and structural damage inspection of Wind turbine blades to reduce the downtime on the maintenance of the offshore wind blades by developing an unmanned automated system (Anisimov et al., 2021). In one of the work packages in this project, we developed an integrated sensor package capable of detecting subsurface defects, particularly spar-cap skin adhesive debonding, in wind turbine blades. Wind blades are constructed using large components composed of relatively low-cost fiber composite materials. In contrast to aerospace standards, these wind blade manufacturing processes often prioritize cost reduction over stringent defect control, as enforcing rigorous defect control measures could result in a high rejection rate (Sørensen et al., 2015). Consequently, a variety of manufacturing defects are anticipated in wind blades. Roach et al. (2017) identified common flaws, damages, and irregularities post-manufacturing that the industry seeks to detect, including thickness variations, disbonds (including kissing disbonds), presence or absence of proper adhesive bonds, interply delaminations, incomplete resin transfer leading to dry regions,

gelcoat disbonds, porosity, snowflaking, in- and out-of-plane waviness, and composite fiber fractures/cracks.

During the operational lifespan of wind blades, small defects can evolve into larger damages, posing a threat to the structural integrity of the blade. Additionally, wind blades operate in diverse environments and are exposed to events that can damage the structure. Shohag et al. (2017) categorized in-situ damage modes occurring during operational life into seven types, as outlined in Table 6.2 and Fig. 6.9. Delamination in laminates and adhesively-bonded joints is often deemed the most critical among these damage modes, according to McGugan et al. (2015).

The sensor package was designed to be lightweight and portable, enabling it to be mounted on a crawler robot for efficient inspection of large blades. For this purpose, the ultrasonic method was chosen as the inspection method for subsurface defects in wind turbine blades due to its versatility, high sensitivity, and ability to provide detailed information about defect size and location. Additionally, UT is portable and can be used to inspect large structures quickly. While UT has some limitations, such as its inability to penetrate sandwich structures and the need for coupling material, it is the most promising method for this application due to its combination of advantages and disadvantages.

6.3.5 Hardware selection

A thorough study of available ultrasonic probes was conducted to identify the most suitable type for our application. Phased array ultrasonic probes were found to be

Table 6.2 Typical damage modes of wind turbine blades.

| 1	Formation and propagation of damage in the adhesive layer connecting the skin and main spar flanges, involving skin/adhesive debonding and/or main spar/adhesive layer debonding.
2	Formation and progression of damage in the adhesive layer that joins the up and downwind skins along leading and/or trailing edges, resulting in adhesive joint failure between the skins.
3	Formation and expansion of damage at the interface between face and core in sandwich panels within skins and main spar web, specifically involving sandwich panel face/core debonding.
4	Formation and progression of internal damage in laminates within skin and/or main spar flanges under either tensile or compression loads, driven by delamination induced by a tensile or buckling load.
5	Splitting and fracture of individual fibers within laminates of the skin and main spar, denoting fiber failure in tension and laminate failure in compression.
6	Buckling of the skin caused by damage initiation and growth in the bond between the main spar under compressive load (skin/adhesive debonding induced by buckling, a specific type 1 case).
7	Creation and expansion of cracks in the gelcoat, along with the debonding of the gelcoat from the skin, involving both gelcoat cracking and gelcoat/skin debonding.
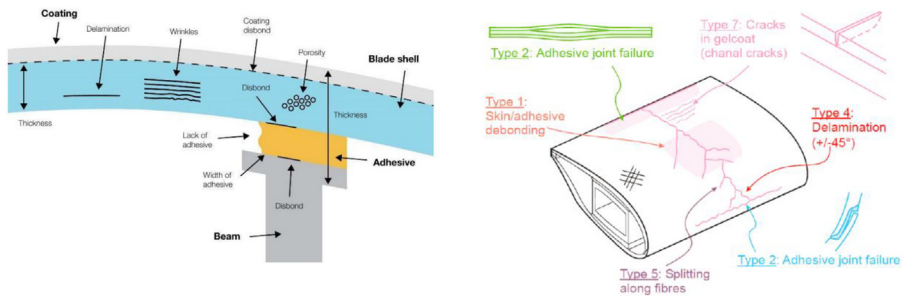
Figure 6.9 Potential defects in the blade structures.
Source: From Lamarre, A. (2017). Improved inspection of composite wind turbine blades with accessible advanced ultrasonic phased array technology. In *15th Asia Pacific Conference for Non-Destructive Testing (APCNDT2017)* (pp. 1−8). (Original work published 2017) and Sørensen et al. (2004). Improved design of large wind turbine blade of fibre composites based on studies of scale effects. (Original work published 2004).

the most appropriate choice due to their ability to provide high-resolution images of subsurface defects as well as their capability for electrical scanning instead of mechanical scanning. Also, electronic control of inspection parameters in the absence of human control is a significant advantage of the ultrasonic phased-array method for our application. The next step for probe selection was choosing the right frequency and for this purpose based on material quality and structural thickness (which was quite inhomogeneous and should cover relatively large thicknesses up to 30 mm) the lower frequency probes were better options despite lower inspection resolution. So, 0.5 MHz and 1 MHz probes were initially down-selected.

A specialized ultrasonic probe designed for in-service pulse-echo inspection is the Roller-probe, which incorporates a PAUT probe encased within a rubber/silicone-coupled and water-filled wheel, as depicted in Figs. 6.10 and 6.11. The rubber tire serves as an acoustic match to water, efficiently transmitting ultrasonic waves into the test component with minimal attenuation. Generally, the probe can operate without a couplant. However, to ensure very good coupling between the probe and the test specimen, a fine water spray is typically applied to the test part.

The PAUT technique, when combined with a wheel probe, is an excellent method for inspecting wind turbine blades. By employing low-frequency transducers, it becomes feasible to examine thick glass fiber structures that exhibit high ultrasound attenuation. When implementing time-corrected gain based on a distance amplitude curve obtained from sources such as flat bottom holes (FBHs) in a representative specimen, a consistent sensitivity can be maintained throughout the entire thickness. The selection process for the probe is outlined in Fig. 6.12.

Based on the target defects and the structure to be inspected, combined with a market analysis, two options for ultrasonic probes were identified:

1. Sonatest phased array wheel-probe 1, 0.5 MHz with 50 elements and 2 mm pitch (see Fig. 6.10).
2. Olympus phased array 1 MHz Rollerform with 128 elements and 1 mm pitch (see Fig. 6.11).

Figure 6.10 Sonatest 0.5 MHz wheel probe.

Figure 6.11 Olympus 1 MHz Rollerform.
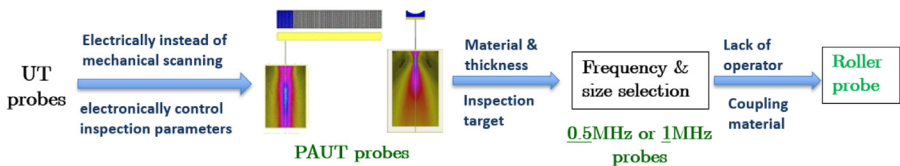*Source*: From OLYMPUS. (2024). https://www.olympus-ims.com/.

Figure 6.12 Probe selection procedure.

6.3.6 Inspection results of reference panels

The inspection results of two reference composite GFRP panels with different levels of curvature and several FBHs with different depths which replicate impact-induced interlaminar delamination, were evaluated. The panels included a reference panel from a section of wind turbine blade skin with a thickness of about 10 mm

(panel IRP-2) and a flat GFRP plate with a thickness of 50 mm (see Fig. 6.13). All of the scan results in this section were achieved from linear scanning with an active aperture size of eight elements and uniform focus depth. Also, an appropriate coupling was achieved by spraying water on the surface of the structure before performing the scan.

C-scan images of the reference panel from a section of wind turbine blade skin (IRP-2) and the B-scan images of the two holes were captured using the Sonatest 0.5 MHz wheel-probe and are depicted in Fig. 6.14.

In Fig. 6.14, "t" refers to the depth of the FDH from the back wall of the panel. Fig. 6.15 summarizes the inspection results for reference panel IRP-2 using *Sonatest* 0.5 MHz probe. The color coding indicates the success rate in detecting and sizing defects: dark green represents successful detection and sizing, light green indicates successful detection but poor sizing, yellow indicates poor detection, and red represents failed detection.

Figure 6.13 The flat glass fiber-reinforced polymer plate with 50 mm thickness.

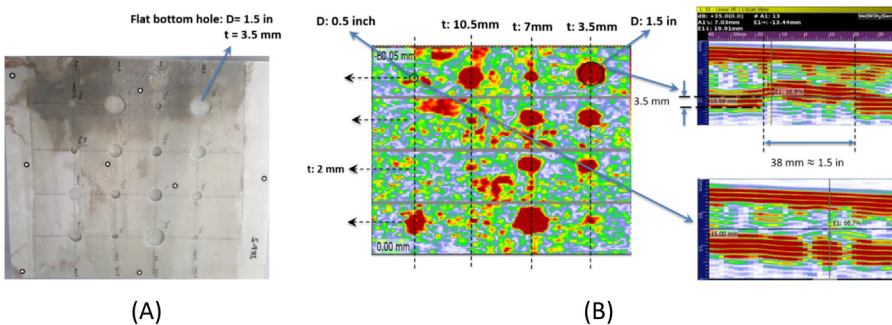(A)   (B)

Figure 6.14 (A) Back surface of panel IRP-2. (B) C-scan image and B-scan image of two FBHs of reference panel IRP-2 captured using Sonatest 0.5 MHz wheel-probe.

depth (mm) / diameter (cm)	2.4	3.4	7.8	10.3	11
3.81		🟩	🟩	🟩	
2.54	🟩	🟩	🟩		🟥
1.9		🟩	🟩	🟩	
1.27	🟥	🟩	🟩	🟩	🟨

Figure 6.15 Statistic map of defect detection in reference panel IRP-2 using Sonatest 0.5 MHz wheel-probe.
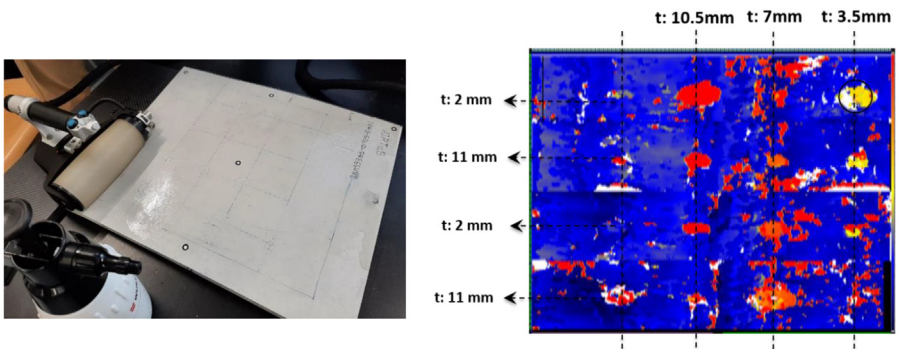

Figure 6.16 C-scan image of reference panel IRP-2 captured by Olympus 1 MHz RollerForm.

As evident from the figure, the 0.5 MHz probe performs well in detecting defects at intermediate depths, but it struggles to detect defects near the surfaces. The C-scan image of reference panel IRP-2 captured by the 1 MHz Olympus probe is presented in Fig. 6.16.

The C-scan image obtained with the 1 MHz probe (Fig. 6.16) exhibits higher noise and attenuation, but it demonstrates better defect detection near the surface than the 0.5 MHz probe. However, the 1 MHz probe struggles to detect defects deeper in the structure compared to the 0.5 MHz probe.

The C-scan images of the 50 mm thick GFRP panel captured using the 0.5 and 1 MHz probes are shown in Figs. 6.17 and 6.18, respectively. While all of the FBHs appear clearly in Fig. 6.17, it is important to note that the panel thickness is greater than the IRP-2 reference panel, and its material quality is superior to that of the reference panels (real turbine blade structures). However, the 1 MHz probe failed to detect the defect at a depth of 30 mm.

Overall, based on the inspection results, the 0.5 MHz Wheel probe was selected as the most suitable combination for this application. The 0.5 MHz probe demonstrated a superior ability to detect defects at intermediate and deeper depths, while
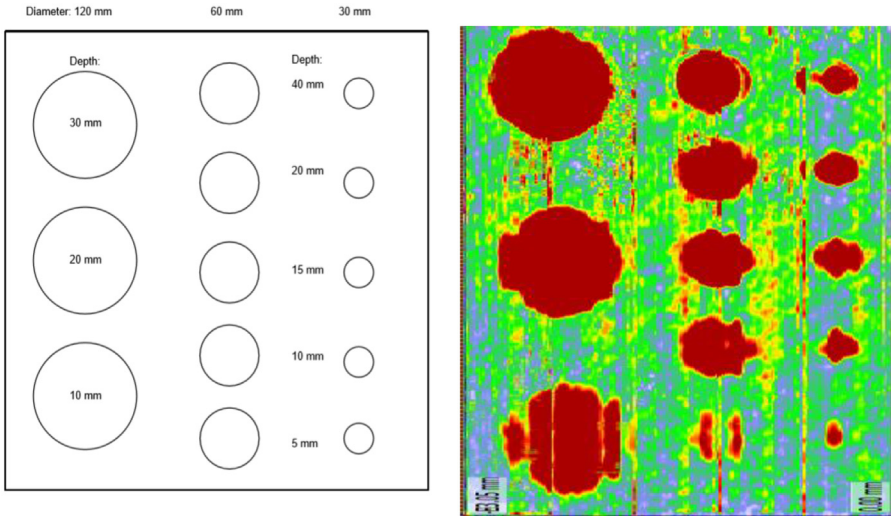
Figure 6.17 C-scan image of glass fiber-reinforced polymer reference panel with 50 mm thickness using Sonatest 0.5 MHz wheel probe.

Figure 6.18 C-scan image of glass fiber-reinforced polymer the reference panel with 50 mm thickness using Olympus 1 MHz wheel-probe.

the 1 MHz probe struggled to penetrate defects at greater depths. Additionally, the 0.5 MHz probe provided better overall image quality compared to the 1 MHz probe, despite its limitations in detecting near-surface defects due to the higher dead-zone area. The choice of the 0.5 MHz probe reflects the prioritization of depth penetration and image clarity over the ability to detect smaller defects and defects near the surfaces.

6.3.7 Evaluation of sensor package and data capturing

After hardware selection, the sensor package was designed and manufactured to carry the whole ultrasonic system and to be integrated into a crawler robot and carried by drone which lands on the wind turbine blade to automatically inspect the subsurface defects. Fig. 6.19 shows the CAD model and the prototype version of the sensor package.
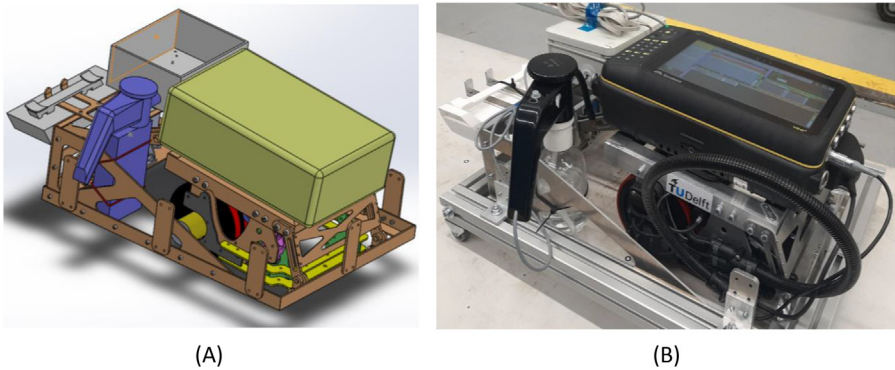

(A)   (B)

Figure 6.19 The CAD model and manufactured prototype of the sensor package.

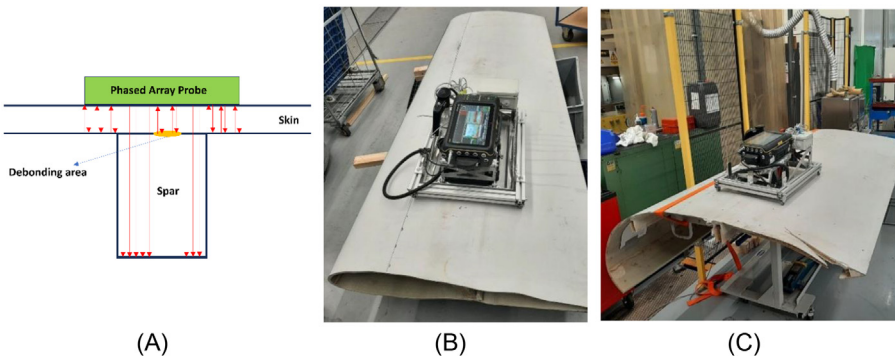(A)   (B)   (C)

Figure 6.20 Performing ultrasonic testing test on different blade sections using the sensor package integrated into the dummy crawler.

After manufacturing and assembling of sensor package evaluation tests were conducted on real blade sections to assess the alignment, coupling, and data acquisition quality. The focus of these tests was the spar cap and skin bonding quality. In order to get a better understanding of the L-scan results, a schematic figure is depicted in Fig. 6.20 to show how ultrasonic waves reflect from different regions of the structure. To validate the scanning results, defects were intentionally introduced in the junction of the spar cap and skin using 1 cm drilling holes and 3.5 cm sawing cuts representing impact damage, as shown in Fig. 6.21. In this figure, the thin and thick black lines indicate the drill holes and sawing cuts, respectively. The red box in Fig. 6.21 indicates the scanning area, while the blue strip indicates the location of spar cap. Fig. 6.22 depicts a typical C-scan and some of its corresponding L-scan results of the spar cap and skin bonding region of a blade section shown in Fig. 6.20C.
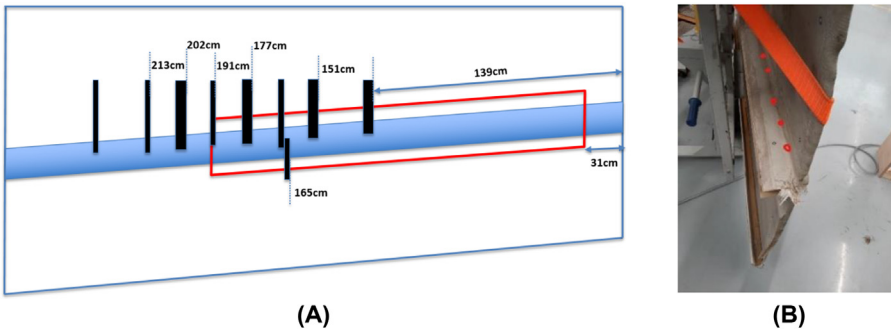

(A)   **(B)**

Figure 6.21 (A) Schematic of the blade section and locations of hand cuts. (B) Side view of hand cut locations.
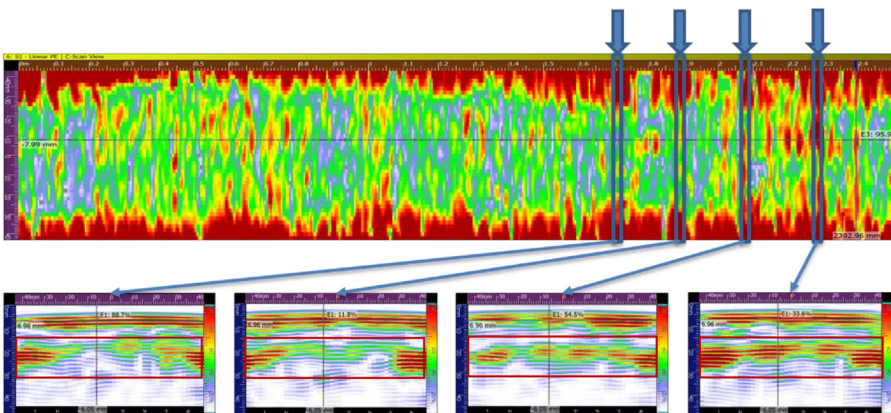

Figure 6.22 The C-scan and some of its corresponding L-scan results of the blade section shown in Fig. 6.20C.
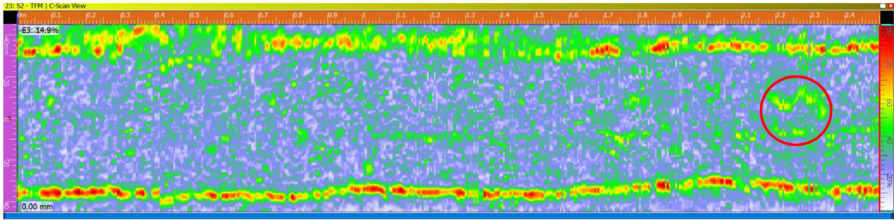
Figure 6.23 Total focusing method result of the full matrix caputre inspection of the blade section shown in Fig. 6.20C with the indication of the largest defect area.

As can be seen in Fig. 6.22, the L-scan results of the suspicious areas in the C-scan, show the debonding area and can give an estimation for its severity based on the amount of reflected ultrasonic energy which is visualized based on the color map. Also, to evaluate the full matrix capturing (FMC) method capability, FMC scans were performed simultaneously. The TFM was applied to the scan signals to analyze the defect locations and features, as shown in Fig. 6.23.

It is apparent from Fig. 6.22 that the presence of numerous voids and porosities in the blade skin leads to noisy signals and C-scan images, making it challenging to identify defects, even if their locations are known. In contrast, the TFM result of the same panel presented in Fig. 6.23 exhibits reduced noise but inferior sensitivity to small defects. As the TFM algorithm uses a positive inference technique, at the defect zone, the maximum amplitude will automatically be normalized to 100% Full-Screen Height. This feature has the advantage that the gain used during acquiring the A-scan data is less critical compared to the conventional phased array.

6.3.8   Performing periodic ultrasonic tests to monitor the structural integrity over time

To assess the capability of the sensor package for structural integrity monitoring, additional hand cuts were introduced on the spar cap and skin bounding region as depicted in Fig. 6.24 by two red thick lines. These cuts were approximately 3.5 cm in width and were intended to simulate defects that could develop over time due to impact or operational stresses. By comparing C-scan images captured before and after inserting new cuts, it is supposed to be possible to identify changes in the structural integrity of the blade. These changes may indicate the presence of new defects or the growth of existing defects. This capability for integrity monitoring can provide valuable insights into the health of the blade and help to ensure its safe operation.

In Fig. 6.25, the C-scan images obtained before and after introducing the new hand cuts are compared. Despite the best efforts to replicate the ultrasonic scan procedure for the second scan, it is evident from the image that discrepancies exist in the scanning conditions, such as the scanning path, coupling pressure, and moisture levels. These variations hinder a straightforward comparison of the C-scans to
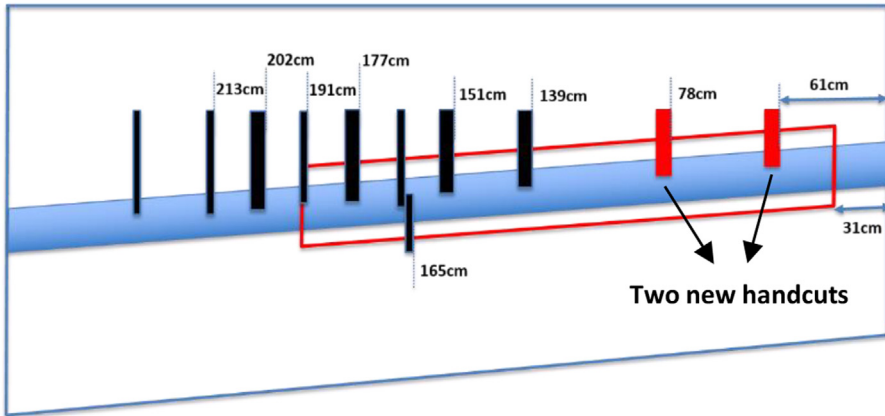
Figure 6.24 Schematic of the blade section and the locations of the additional two hand cuts distinguished by red color.
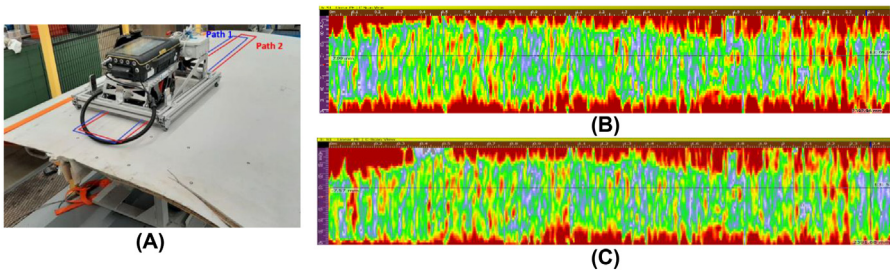

Figure 6.25 (A) Difference between the scanning paths, (B) C-scan of the blade section before placing new hand cuts, and (C) C-scan of the blade section after placing the new hand cuts.

identify changes in the blade's structural integrity. To address this difficulty and enable a more accurate comparison, a data-fitting algorithm was employed. This algorithm analyzes the two C-scan images and identifies similar features between them. By comparing the relationships between these features in the two scans, it is possible to detect subtle changes in the blade's condition, even in the presence of varying scanning conditions.

As is clear in Fig. 6.25, the indication of these two new defects with such a size is barely visible (or it might be considered invisible) by comparison of the two C-scan results and it takes a lot of effort and time to find two 3.5 cm cut damage, even if their location is known. This problem can greatly increase the cost of expert human resources when the amount of data increases significantly. To ease the procedure of comparison, a data-fitting algorithm is developed which is explained below.

6.3.9 Developing the data-fitting algorithm

To facilitate the comparison procedure, a data-fitting algorithm was developed that utilizes only A-scan ultrasonic signals and does not require additional information. This algorithm automatically identifies shifting patterns in the signals of the new scan (due to the deviation of the scanning path, and the difference in the transducer coupling quality) and compares them to corresponding signals in previous scans. Fig. 6.26 demonstrates a simple comparison resulting from subtracting individual signals without performing the mentioned data fitting algorithm. This subtraction method introduces substantial noise and irrelevant defect information, hindering accurate defect identification.

The first step in comparing ultrasonic scans is to identify the best correlation between the two-dimensional scans. Fig. 6.27 illustrates how the C-scan result is constructed from multiple L-scans. To determine the shifting pattern in the length direction of C-scan results, we selectively extracted 5% of L-scans distributed throughout the length of the C-scan results. For each individual L-scan, it was compared with the corresponding L-scan in the second C-scan result and its adjacent L-scans to identify the L-scan that exhibited the strongest correlation. This process was repeated for all selected L-scans across the length of the C-scan. The most frequently observed shift value among these correlations was deemed the overall shift value for the C-scan result.

Following the determination of the shift value in the path direction of the second inspection (which can refer to the shifting of the starting point of the scanning path in the x direction), it proceeded to identify the misalignment value for each individual L-scan. For this purpose, each L-scan was compared from the first inspection to its corresponding counterpart in the second inspection. for each pair of L-scans in
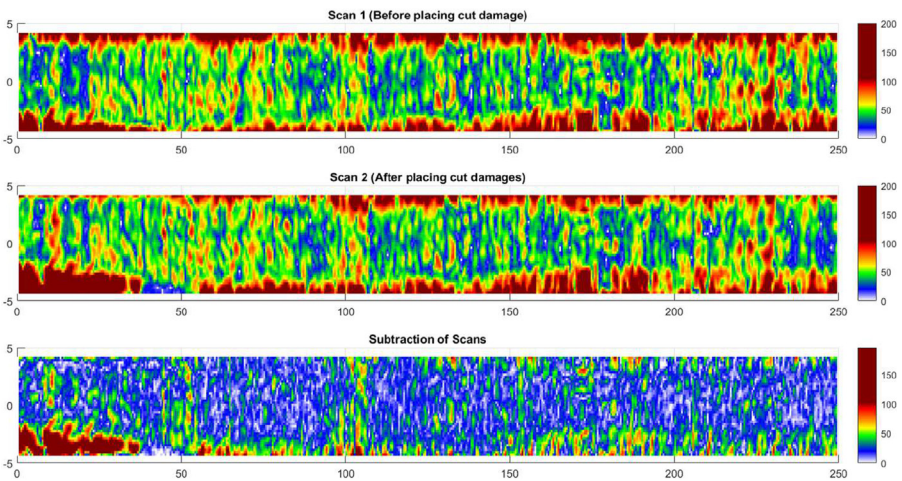

Figure 6.26 Difference between the scanning path of the first and second Ultrasonic inspection.
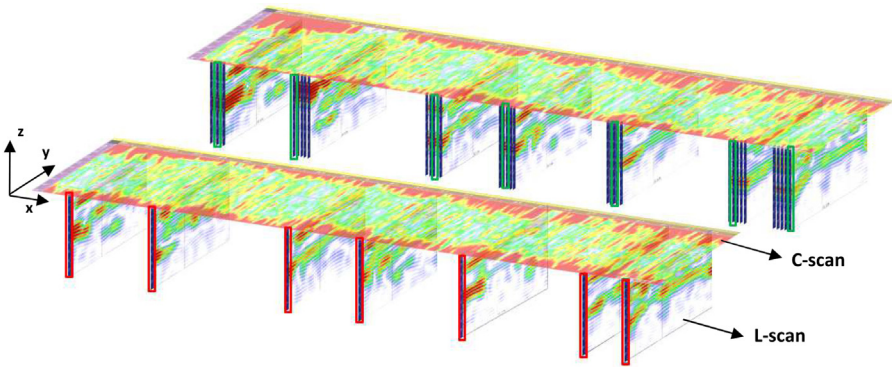
Figure 6.27 The 3D shape of C-scan results which is composed of L-scan results.
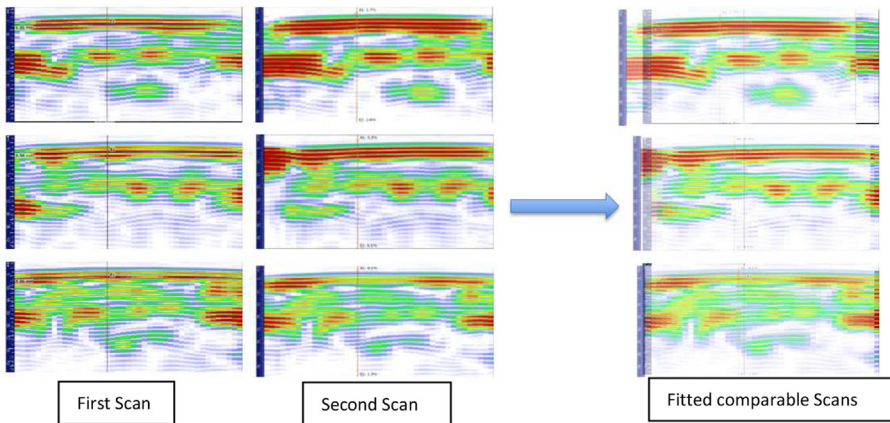

Figure 6.28 The result of the fitting algorithm for each L-scan pair result.

both inspections, the best match of two images was found by defining windows and features and moving the window to find the best cross-correlation between the A-scan signals inside the window and the corresponding signals in the related L-scans. The outcome of this procedure for three representative L-scans is depicted in Fig. 6.28.

After completing this misalignment correction process, it is possible to effectively compare the scanning outcomes automatically. The most straightforward approach involves subtracting corresponding signals from the same locations and points, as shown in Fig. 6.29. This subtraction operation effectively highlights the differences between the two C-scan images, enabling the identification of potential defects or changes in the structural integrity.

While Fig. 6.29 clearly reveals the locations of the hand-cut damages, the wrong sign of anomalies persists, potentially attributable to variations in the coupling
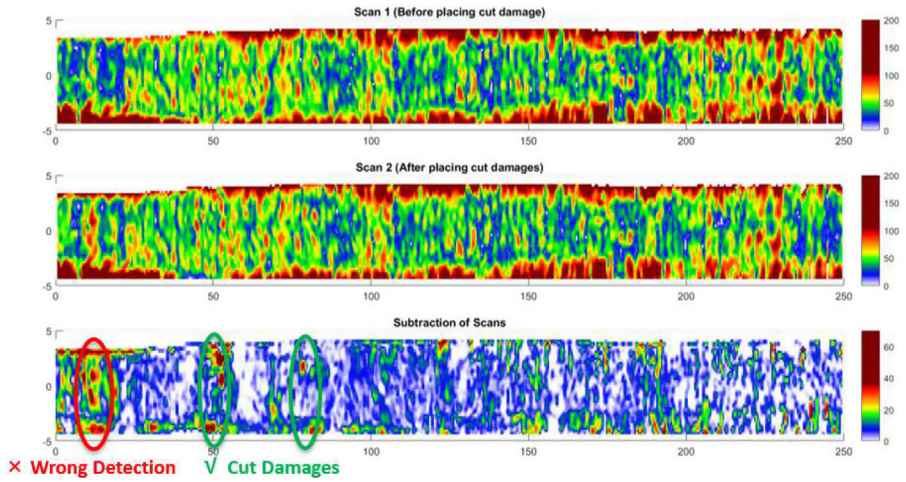
Figure 6.29 Comparison of the inspection results after performing data fitting.

condition between the probe and the surface. These discrepancies primarily result in disparities in the ultrasonic energy transmitted to the structure. To address this issue, individual signals are normalized based on the energy of each signal in the Far-field domain. To calculate the nearfield distance one can use Eq. (6.3) (Bossi & Giurgiutiu, 2015):

$$N = \frac{A^2}{4\lambda}, \lambda = \frac{v}{f}, A = np \tag{6.3}$$

where $\lambda, v,$ and f are the wavelength, wave velocity, and wave frequency respectively. Also, A is the active aperture consisting of n active elements with a pitch size of p. As we use the roller probe, inside the probe, there is a water path ($L_{\text{waterpath}}$) between the probe and the structure, therefore, the nearfield distance in the blade structure is calculated as

$$N_{\text{Composite after waterpath}} = N_{\text{composite}} - L_{\text{waterpath}} \times \frac{v_{\text{water}}}{v_{\text{composite}}} \tag{6.4}$$

For the used probe and structure, the near field distance in the structure is about 8 mm which is considered in the energy normalization process. After normalizing the ultrasonic signals based on their far-field domain energy (which can be determined by knowing the near-field distance), the comparison of the two inspections is depicted in Fig. 6.30.

As evident in Fig. 6.30, the two hand-cut damages introduced between inspections are clearly visible in the subtracted signal image. It's important to emphasize that for the sake of simplicity, the most basic approach for signal comparison, which involved subtracting time-amplitude signals was employed. However, there
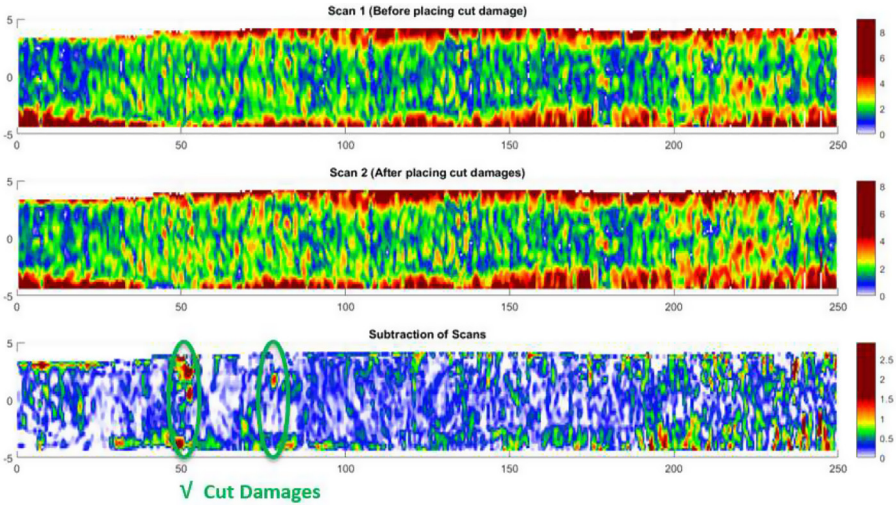
Figure 6.30 Comparison of the inspection results after performing data fitting and energy normalization.

is ample room for algorithm enhancement by incorporating frequency-domain signal features and correlation-based techniques. These advancements could refine the comparison process, enabling more accurate and precise defect identification.

6.4   Conclusions and future directions

This chapter has explored the area of damage assessment in thick composite laminates utilizing PAUT. We started our chapter with an introduction to fundamental theories, encompassing elastic waves, attenuation and impedance, refraction, mode conversion, and the scattering of waves from defects. Special emphasis was placed on the capacity of UT to discern various damage mechanisms within composite laminates. The subsequent section provided a detailed exploration of PAUT, encompassing principles, and basics, including probes, software, and control mechanisms. We extended our study to various PAUT data acquisition methods, such as FMC, linear scanning, sectoral scanning, raster scanning, and various ultrasonic views, followed by introducing the beamforming methods employed in PAUT. In the next section, the practical application of PAUT for damage assessment was illustrated by a case study focusing on sparcap and skin debonding detection in wind turbine blades. This section also explained the hardware selection, inspection results of reference panels, evaluation of the PAUT probes and sensor package, and the development of a data fitting algorithm as s postprocessing technique. The showcased results show that PAUT stands as an effective tool for damage assessment in thick composite laminates and also proves how such a postprocessing technique can enhance the capability of this method for the

inspection of complex and noisy structures. Looking ahead, future directions in this field may involve advancements in probe technologies, software enhancements for more efficient data analysis, as well as the integration of artificial intelligence for automated defect recognition and real-time monitoring. In addition, contributing to the establishment of standardized procedures and validation methodologies for applying PAUT in different composite structures has great importance.

In conclusion, the combination of theoretical foundations, PAUT principles, and practical case studies has laid a robust foundation for the effective use of PAUT in assessing damage in thick composite laminates. The suggested future directions aim to further refine and expand the capabilities of PAUT as a powerful tool in NDE. ACKNOWLEDGEMENTS The AIRTuB project (Automatic Inspection and Repair of Turbine Blades) is being carried out with a Top Sector Energy subsidy from the Ministry of Economic Affairs of the Netherlands.

Acknowledgements

References

Anisimov, A. G., Beukema, R., Hwang, J., Nijssen, R., & Groves, R. M. (2021). AIRTuB: towards automated inspection of leading edge erosion of wind turbine blades by shape analysis. In *Multimodal sensing and artificial intelligence: Technologies and applications II, Vol. 11785* (p. 117850W). SPIE.

ASTM E2533-09 Standard Guide for Nondestructive Testing of Polymer Matrix Composites Used in Aerospace Applications. (2009). *Annuual B. ASTM Standard.* Available from https://doi.org/10.1520/E2533-09.part.

Blitz, J., & Simpson, G. (1995). *Ultrasonic methods of non-destructive testing* (2). Springer Science & Business Media.

Bossi, R. H., & Giurgiutiu, V. (2015). *Nondestructive testing of damage in aerospace composites. Polymer composites in the aerospace industry* (pp. 413−448). United States: Elsevier Inc. Available from http://www.sciencedirect.com/science/book/9780857095237, https://doi.org/10.1016/B978-0-85709-523-7.00015-3.

Cawley, P. (2006). Inspection of composites−current status and challenges. In *Proceedings of 9th ECNDT*.

Dubee, N., & Michael, D. C. H. (2007). *Advances in phased array ultarasonic applications. Technical note, Technical communications services.* Olympus NDT.

Fahr, A. (2014). *Aeronautical applications of non-destructive testing.* DEStech Publications.

Heida, J. H., & Platenkamp, D. J. (2011). Evaluation of non-destructive inspection methods for composite aerospace structures. NDT in progress 2011. In *6th International Workshop of NDT Experts, Proceedings* (pp. 67−78) Prague, Czech Republic, 9788021443396.

Henrich, R., & Schnars, U. (2006). Applications of NDT Methods on Composite Structures in Aerospace Industry. Conference on Damage in Composite Materials 2006, September in Stuttgart, Germany. *e-Journal of Nondestructive Testing*, *11*(12). Available from https://www.ndt.net/?id = 4180.

Huang, R. (2006). Ultrasonic modeling for complex geometries and materials. *Iowa State University*.

Ibrahim, M. E. (2014). Nondestructive evaluation of thick-section composites and sandwich structures: A review. *Composites Part A: Applied Science and Manufacturing*, *64*, 36−48. Available from https://doi.org/10.1016/j.compositesa.2014.04.010.

Krautkrämer, J., & Krautkrämer, H. (2013). *Ultrasonic testing of materials*. Springer Science & Business Media.

Lamarre, A. (2017). Improved inspection of composite wind turbine blades with accessible advanced ultrasonic phased array technology. In *15th Asia Pacific conference for non-destructive testing (APCNDT2017)* (pp. 1−8).

Lopez-Sanchez, A. L., Kim, H. J., Schmerr, L. W., & Gray, T. A. (2006). Modeling the response of ultrasonic reference reflectors. *Research in Nondestructive Evaluation*, *17*(2), 49−69. Available from https://doi.org/10.1080/09349840600689459.

Mailloux, R. J. (1982). Phased array theory and technology. *Proceedings of the IEEE*, *70*(3), 246−291. Available from https://doi.org/10.1109/proc.1982.12285.

McGugan, M., Pereira, G., Sørensen, B. F., Toftegaard, H., & Branner, K. (2015). Damage tolerance and structural monitoring for wind turbine blades. *Philosophical Transactions of the Royal Society A: Mathematical, Physical and Engineering Sciences*, *373*(2035). Available from https://doi.org/10.1098/rsta.2014.0077.

Moon, C. J., Whateley, M. K., & Evans, A. M. (2006). *Introduction to mineral exploration (No. Ed. 2)*. Blackwell Publishing.

Namkung, M., Wincheski, B., & Padmapriya, N. (2016). *NDT in the aircraft and space industries*. Elsevier BV. Available from https://doi.org/10.1016/b978-0-12-803581-8.01940-8.

Nightingale R, Phased array. Case study, Radiopaedia.org (Accessed on 15 May 2024), 26 Jul 2017. Available from https://doi.org/10.53347/rID-54646

Nokhbatolfoghahai, A., Navazi, H. M., & Groves, R. M. (2020). Using the hybrid DAS-SR method for damage localization in composite plates. *Composite Structures*, *247*, 112420.

Ogilvy, J. A., & Temple, J. A. G. (1983). Diffraction of elastic waves by cracks: Application to time-of-flight inspection. *Ultrasonics*, *21*(6), 259−269. Available from https://doi.org/10.1016/0041-624x(83)90058-6.

Olympus Phased Array Tutorial, Learn About Ultrasonic Phased Array. (2023) https://www.olympus-ims.com/en/ndt-tutorials/phased-array/. (accessed December 2023).

Ono, K. (2020). A comprehensive report on ultrasonic attenuation of engineering materials, including metals, ceramics, polymers, fiber-reinforced composites, wood, and rocks. *Applied Sciences*, *10*(7). Available from https://doi.org/10.3390/app10072230.

Perrot, V., Polichetti, M., Varray, F., & Garcia, D. (2021). So you think you can DAS? A viewpoint on delay-and-sum beamforming. *Ultrasonics*, *111*. Available from https://doi.org/10.1016/j.ultras.2020.106309.

Roach, D., Rice, T., & Paquette, J. (2017). Probability of detection study to assess the performance of nondestructive inspection methods for wind turbine blades.

Schmerr, L. W. (2003). *Fundamentals of ultrasonic phased arrays* (215). Springer International Publishing.

Schmerr, L. W. (2016a). *Fundamentals of ultrasonic nondestructive evaluation* (122). Springer.

Schmerr, L. W. (2016b). *Fundamentals of ultrasonic nondestructive evaluation: A modeling approach*. Springer.

Schmitz, V., Chakhlov, S., & Müller, W. (2000). Experiences with synthetic aperture focusing technique in the field. *Ultrasonics*, *38*(1−8), 731−738. Available from https://doi.org/10.1016/s0041-624x(99)00219-x.

Shohag, M. A. S., Hammel, E. C., Olawale, D. O., & Okoli, O. I. (2017). Damage mitigation techniques in wind turbine blades: A review. *Wind Engineering.*, *41*(3), 185−210. Available from https://doi.org/10.1177/0309524X17706862, http://wie.sagepub.com/content/by/year.

Smith, R. A., Mukhopadhyay, S., Lawrie, A., & Hallett, S. R. (2013). Applications of ultrasonic NDT to aerospace composites. In *5th international sSymposium of NDT aerospace*.

Song, T. K., & Greenleaf, J. F. (1994). Ultrasonic dynamic focusing using an analog FIFO and asynchronous sampling. *IEEE Transactions on Ultrasonics, Ferroelectrics, and Frequency Control*, *41*(3), 326−332. Available from https://doi.org/10.1109/58.285466.

Sørensen, Bent F., Helmuth Langmaack Toftegaard, Malcolm McGugan, Gilmar Ferreira Pereira, and Kim Branner. "Very large wind turbine rotor blades require damage tolerance and damage monitoring." In *EWEA Offshore 2015 Conference*. 2015.

Sørensen, B. F., Joergensen, E., Debel, C. P., Jensen, H. M., Jacobsen, T. K., & Halling, K. (2004). Improved design of large wind turbine blade of fibre composites based on studies of scale effects (Phase 1). Summary report. Chicago.

Steinchen, W., Yang, L., Kupfer, G., & Mäckel, P. (1998). Non-destructive testing of aerospace composite materials using digital shearography. *Proceedings of the Institution of Mechanical Engineers, Part G: Journal of Aerospace Engineering*, *212*(1), 21−30. Available from https://doi.org/10.1243/0954410981532108.

Su, Z., & Ye, L. (2009). Fundamentals and analysis of Lamb waves. *Lecture Notes in Applied and Computational Mechanics*, *48*, 15−58. Available from https://doi.org/10.1007/978-1-84882-784-4_2.

Tittmann, B. R. (1983). Scattering of elastic waves from simple defects in solids, a review. *Wave Motion*, *5*(4), 299−306. Available from https://doi.org/10.1016/0165-2125(83)90019-7.

Tremblay, D. R. (2012). *Development and validation of a full matrix capture solution* (pp. 457−466).

Von Ramm, O. T., & Smith, S. W. (1983). Beam steering with linear arrays. *IEEE Transactions on Biomedical Engineering*, *30*(8), 438−452. Available from https://doi.org/10.1109/TBME.1983.325149.

Williams, J. C., & Starke, E. A. (2003). Progress in structural materials for aerospace systems. *Acta Materialia*, *51*(19), 5775−5799. Available from https://doi.org/10.1016/j.actamat.2003.08.023.

Yin, J.-F., Bai, Q., & Zhang, B. (2018). Methods for detection of subsurface damage: A review. *Chinese Journal of Mechanical Engineering*, *31*(1). Available from https://doi.org/10.1186/s10033-018-0229-2.

Zhang, J., Drinkwater, B. W., Wilcox, P. D., & Hunter, A. J. (2010). Defect detection using ultrasonic arrays: The multi-mode total focusing method. *NDT and E International*, *43*(2), 123−133. Available from https://doi.org/10.1016/j.ndteint.2009.10.001.